Implementation of a fast time-domain processor for FMCW Synthetic Aperture Radar data

Frioud, Max ; Wellig, Peter ; Stanko, Stephan ; Meier, Erich

DOI: https://doi.org/10.1117/12.2194331

Implementation of a fast time-domain processor for FMCW Synthetic Aperture Radar data

Max Frioud*[a], Peter Wellig[b], Stephan Stanko[c], Erich Meier[a]
[a]Remote Sensing Laboratories, University of Zurich, Zurich, Switzerland
[b]Science and Technology Department, armasuisse, Thun, Switzerland
[c]Fraunhofer Institute for High Frequency Physics and Radar Techniques FHR, Wachtberg, Germany

ABSTRACT

For the purpose of getting sensitive information relevant to civil or military security, high-resolution airborne Synthetic Aperture Radar (SAR) provides the possibility to organize missions at short notice regardless of the daylight and of the weather conditions. The use of compact millimeter-wave FMCW SAR systems allows reaching these goals more safely and at lower cost using unmanned lightweight platforms. As a counterpart these platforms are relatively unstable, making the data-processing more difficult. In order to reach optimum focusing quality also in unfavorable flight conditions or for highly non-linear tracks we developed a fast Time-Domain Processor that relies on parallelization using the GPU resources. A production areal processing rate as high as 6 km^2/h using 20 cm ground pixel spacing on a single PC station was achieved. The processing quality and efficiency is demonstrated using real data from the MIRANDA35 Ka-band SAR system.

1. INTRODUCTION

In the context of surveillance of sensitive areas for military or civil applications, imaging using airborne FMCW SAR from lightweight and possibly unmanned platforms presents a very interesting compromise between required resolution, low payload weight and power consumption, as well as the flexibility to image several sites irregularly distributed over large areas within a short time frame. In the last years, many airborne sensors aiming high resolution imaging have exploited the millimiter-wave atmospheric windows at Ka- and W-bands [1]-[4], which are particularly aimed at revealing small terrain structures.

For extracting the best information from such systems, the accuracy requirements for the processing of both navigational data and SAR data are very high [5]. Generally speaking, SAR processors fall into two classes, namely frequency-domain and time-domain. Frequency-domain processors are computationally the less intensive of the two, but they suffer several drawbacks: (a) they require a motion compensation step that performs ideally only as long as the sensor trajectory does not deviate too much from a straight line, (b) as they treat 2D collections of pixels as a whole, they are very demanding on RAM, and (c) strategies to properly deal with strong variations of the Doppler-Centroid in the range and/or in the azimuth dimensions further increase the demand on RAM and considerably reduce their efficiency.

In order to retain optimal quality also for highly non-linear trajectories as well as possible fast variations of the platform attitude, we developed a Time-Domain processor dedicated to the focusing of airborne FMCW SAR data. It outputs geocoded products in map geometry. Despite the intense computational load, a high efficiency is reached thanks to (a) an efficient focusing algorithm [6], (b) process parallelization on a Graphics Processing Unit (GPU) using CUDA©®, (c) efficient partitioning of the illuminated area, and (d) efficient implementation of computationally heavy operations.

In addition to its robustness and efficiency, the processor already includes a precise correction scheme for the relative radiometric calibration. For SAR imaging, optional single-look or multi-look processing modes are already integrated in the processor. For application of Ground Moving Target Indication the processing is extended outside the system beam-width to provide exo-clutter signatures from moving objects: this mode is typically applied to azimuth segments much smaller than the full aperture, allowing e.g. single channel tracking of vehicles by analyzing time series of images [7].

The performance of the processor was assessed using real SAR data acquired by the Ka-band system MIRANDA35 [8] during measurement campaigns in Switzerland by analyzing the signatures from corner reflectors.

*max.frioud@geo.uzh.ch; phone +41 44 635 51 97; fax +41 44 635 68 46; www.geo.uzh.ch/en/units/rsl

SAR Image Analysis, Modeling, and Techniques XV, edited by Claudia Notarnicola, Simonetta Paloscia, Nazzareno Pierdicca, Proc. of SPIE Vol. 9642, 96420B
 · doi: 10.1117/12.2194331

2. METHOD

I. Efficient Focusing Algorithm

The chosen algorithm for focusing the FMCW SAR data is an approximation of the Time Domain Correlation (TDC) Algorithm. The de-chirped RAW data depend on the ramp time and on the azimuth time. In discrete form, it is expressed as follows

$$s(m,n) = \int_R \alpha(\boldsymbol{x}) A(\boldsymbol{x},m,n) e^{-2\pi i \varphi(\boldsymbol{x},m,n)} d\boldsymbol{x} \tag{1}$$

Here m, n denote the indices to the discrete time variables t_a (azimuth) and t_r (ramp), $\alpha(\boldsymbol{x})$ is the terrain complex reflectivity at some point $\boldsymbol{x}$ in the illuminated region R, A is an amplitude function including the effects of the range-spread loss and of the antenna pattern, and φ is the phase function that carries the information needed for coherent processing which is given by

$$\varphi(\boldsymbol{x},m,n) = (K \cdot \tau(\boldsymbol{x},m,n) - F) \cdot t_r(n) + f_0 \cdot \tau(\boldsymbol{x},m,n) - \frac{K}{2} \cdot \tau^2(\boldsymbol{x},m,n) \tag{2}$$

where f_0 is the carrier frequency, F is the demodulation frequency, K is the slope of the ramp and $\tau(\boldsymbol{x},m,n)$ is the round-trip time-delay from the radar to a scatterer located at $\boldsymbol{x}$ at the physical time $t(m,n) = t_a(m) + t_r(n)$. The TDC solution to (1) is to correlate the measured signal with the expected one from a point scatterer at $\boldsymbol{x}$, as follows

$$\alpha(\boldsymbol{x}) = \sum_{m,n} W(\boldsymbol{x},m,n) \cdot s(m,n) \cdot s_{\boldsymbol{x}}^*(m,n) \tag{3}$$

where W is a tapering window used for reducing the side-lobes and $s_{\boldsymbol{x}} = e^{-2\pi i \varphi(\boldsymbol{x},m,n)}$. A direct implementation of (3) is numerically way too intensive for processing full scenes from high-resolution SAR data. Thus some approximations are needed. As exposed in [6], under some conditions it is possible to transform (3) in such a way that the coherent integration over the ramp-time t_r can be reduced to a Fourier Transform. The validity of this approach was demonstrated using real SAR from the system COBRA SAR system [6], and was assessed using simulated data of point targets for the system parameters of MIRANDA35 used in this work [8]. Thus the core of the focusing with this simplified version of TDC relies on following operations:

(a) 1D FFT in the t_r direction.

(b) 1D complex interpolation (along the slant range dimension) to the evaluation points, depending on the system parameters, the distances and the approach velocities between radar and backscattering elements.

(c) phase function multiplication.

(d) coherent integration over the azimuth dimension.

For high performance the operations (a) and (b) were implemented as a combination of zero-padding prior to FFT for data-upsampling by a factor 4 and a Keys' cubic spline interpolation performed separately on real and imaginary parts of the FFT output.

A scheme of the overall processing chain as applied to MIRANDA35 SAR data is presented in Figure 1. In this Figure the left column below "SAR raw data" shows the SAR part of the processing chain, while the right part shows the used meta-data and the processing steps required for the evaluation of the geometrical inputs to the SAR part.

A pixel-based relative radiometric correction is fully integrated to this processing scheme. It corrects for the effects of range-spreading loss, antenna beam-patterns in azimuth and elevation as well as tapering windows used for the side-lobe reduction, in the same way as described in [9]. The extra work load needed for this correction is relatively limited because it uses mostly the same variables as those needed for the SAR focusing itself.

II. Process parallelization on GPU

As all Time-Domain SAR processing, the focusing method exposed above is extremely well suited to parallelization, since (a) the processing for the various ground pixels are independent on each other and (b) the processing is separable in the range and azimuth dimensions, i.e. it never requires a 2D dataset to be processed at once, thus limiting considerably the required RAM as well as the amount of data to be transferred to the GPU. The segment of processing running on GPU is represented in Figure 1.

The parallelization is implemented in C++ using the Compute Unified Device Architecture (CUDA) from NVIDIA©®. As the way the processing on GPU is split among various kernels does significantly influence the efficiency, efforts have been focused to optimize this partitioning.

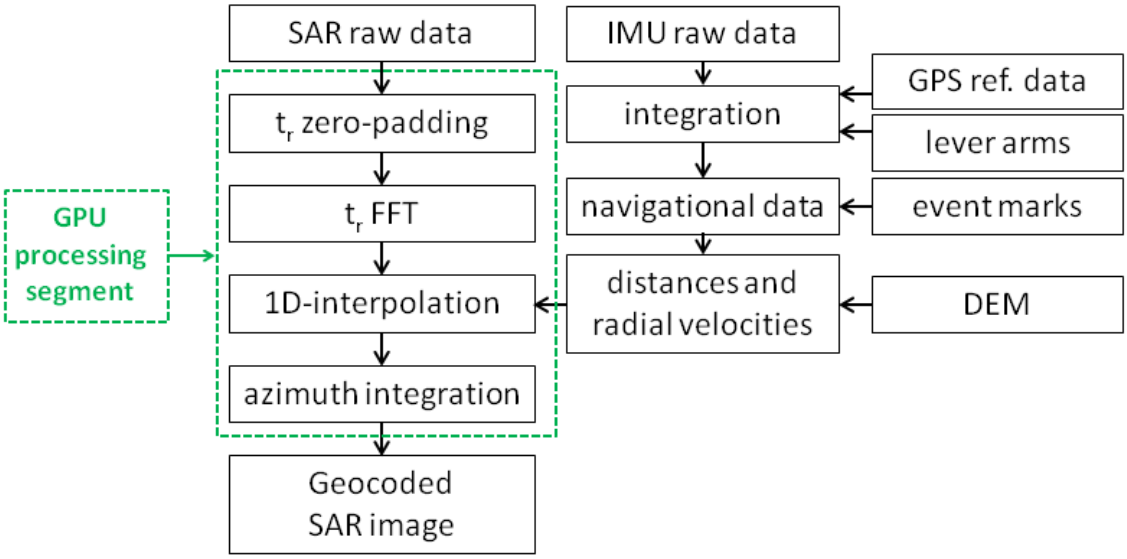

Figure 1. Overall processing scheme for FMCW airborne SAR data using the implemented method.

III. Efficient partitioning of the illuminated area

In order to deal with the large amount of ground pixels for processing a typical airborne data-take in high-resolution (pixel spacing of a few dm), the illuminated area is partitioned into sets over which the processing operates sequentially. The illuminated area is first defined by range constraints determined by the SAR system as well as angular constraints defined by the platform position and attitude as well as by the antenna look direction and its angular beam-width in both azimuth and elevation and by the Digital Elevation Model (DEM). Unlike for pulsed SAR, each pixel of a given ramp of raw data contains information about the whole swath for FMCW SAR. Therefore it is of advantage to group pixels in the whole swath sharing almost the same azimuth time corresponding to the maximum beam illumination (since these pixels share the same operations (a)-(b) described in I.). A way to reduce redundancy in the operations is to group the pixels according to their processed azimuth time window. The illuminated region is partitioned in small squared cells a few meters in size hereafter referred to as mini-tiles. The processed azimuth time window for the centers of all the mini-tiles are evaluated from the navigational data and the mini-tiles are sorted according to their azimuth start-time. Finally the sets used for sequential processing are defined as contiguous segments of fixed size from this sorted list.

IV. Efficient implementation of computationally heavy operations

When irrelevant to the image quality, some operations on GPU are performed in single precision while most of the operations are performed in double precision. This is particularly the case for some trigonometric operations needed for the radiometric correction of the antenna, for which very high precision is not needed.

Attempts to use Look-Up Tables (LUT) for replacing certain operations (such as the square root) failed because the time of access to the LUT turned out to be larger than using the built-in functions.

3. RESULTS

The implemented method was tested using real SAR data from the experimental system MIRANDA35 [3]. It is a compact Ka-band system, which offers high flexibility thanks to a wide choice of possible waveforms for SAR data-takes (bandwidth ranging from 150 MHz to 1 GHz, mid-range from about 1000 m to 5000 m, and swath-width from about 500 m to 2000 m). For the Swiss measurement campaigns, it was mounted onboard an optionally piloted aircraft CENTAUR, which is basd on a highly modified Diamond DA42 multi-purpose platform. Besides the SAR sensor, an integrated high resolution optical camera is looking in the same direction as the radar. Both sensors provide simultaneous real-time observations thanks to a very fast onboard SAR processor and a digital link to a ground control station [10][11].

Figure 2 presents the results from a Point Target Analysis (PTA) applied to the SAR signature of a corner reflector which was deployed on concrete. For the analysis, the data was focused using a ground pixel spacing of 0.4 cm, the amplitude image was up-sampled to 0.2 cm and no tapering windows were used for side-lobe reduction. Under nominal conditions the expected system's azimuth resolution is about 10 cm, but it falls down to 7.8 cm for this particular case when accounting for the variation of the platform attitude during the aperture. From the PTA an azimuth resolution of 7.5 cm was measured, which is very consistent with the expectation. In the range direction the expected and measured values (25.0 cm and 22.7 cm) also demonstrate good consistency. The one-sided peak-side-lobe ratios in range (-10.5 dB and -11.3 dB) are a bit worse than expected (-13.26 dB), a point which needs further investigation. Overall the PTA demonstrates a very high focusing quality.

Figure 3 presents an example of a SAR image from a curved trajectory, typically well suited for traffic monitoring along highways. As the radar bandwidth is 600 MHz, it was processed with a ground pixel spacing of 20 cm. Thanks to the radiometric calibration, the image intensity distribution is smooth and has a reduced dynamic range. The far range region in the curve has a poor signal-to-noise ratio due to the combination of the platform banking and the use of a fixed antenna. The image is laid over an orthophoto from the Swiss Federal office of topography.

Figure 4 presents an extract of a SAR image of a rural area from a linear trajectory. As the radar bandwidth is 1000 MHz, it was processed with a ground pixel spacing of 15 cm. Due to their movement during the aperture time the trees appear blurred. Otherwise the image has high contrast and excellent focusing quality.

Figure 5 is an example of the use of multi-look processing. The left image is obtained from a full-aperture processing (using 80% of the nominal beam-width), while the right image is the result from incoherently averaging several images produced by processing successive azimuth segments of the raw data (the number of looks is about 4). One clearly notices the much higher side-lobes from strong scatterers such as roof edges in the multi-look image. One also observes the reduction of speckle effect thanks multi-looking especially in the grass areas. Thanks to the pixel-based radiometric correction adapted to multi-look processing, one also notices the absence of any azimuth pattern that often affect multi-look images at the borders of the single sub-aperture images.

For the efficiency tests, we utilize current commercial off-the-shelf components as listed in Table 1 (for additional details refer to manufacturer data sheets). The results of a test are shown in Table 2. Four data-takes from the 2014 campaign were chosen for this test: three 600 MHz with different system settings according to the different flight altitudes, and one 300 MHz with the same altitude and swath-width than the third one. In all cases the processed azimuth beam-width was the same, namely 80% of the antenna nominal value. Since the mount-depression angle of the antenna is fixed (35 deg), the aperture length is proportional to the altitude. The poorer areal processing rates with increasing altitudes are consistent with this observation (last row of Table 2, Cases 1 to 3). The comparison of Case 3 and Case 4 demonstrates that the speed-up factor obtained by increasing the pixel-spacing does not simply scale with the inverse of the ratio of pixels' areal densities.

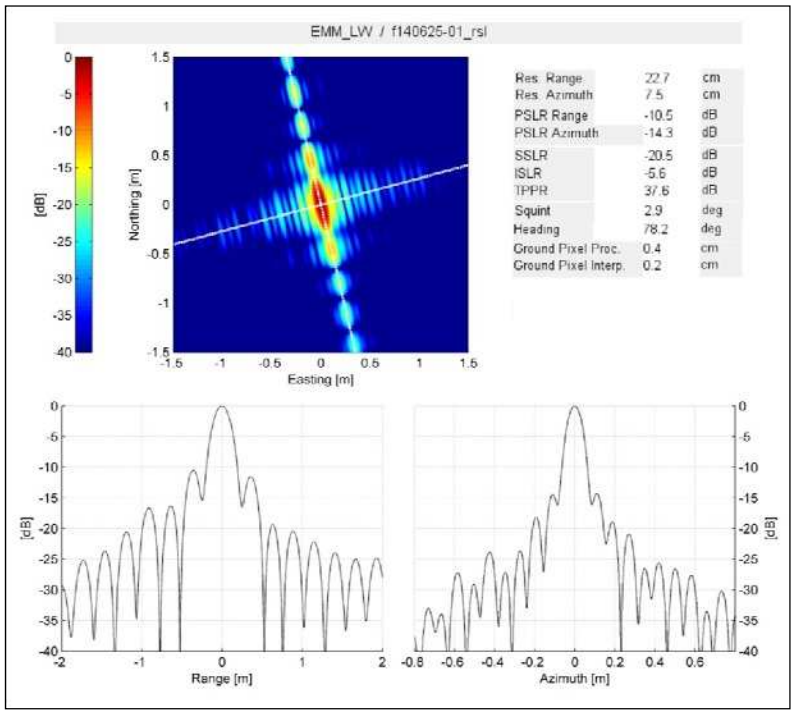

Figure 2. Point target analysis applied to the SAR signature of a corner reflector.

Figure 3. SAR image from a 600 MHz data-take. Size: 3350 m x 1860.

Figure 4. Extract of SAR image from a 1000 MHz data-take. Size: 495 m x 300 m.

(a) Single-look

(b) Multi-look (4 looks)

Figure 5. Extract of SAR images processed with 20 cm pixel spacing. Size: 210 m x 180 m.
Illumination direction: toward N-NW.

Table 1. Computing platform characteristics used for the efficiency test.

Properties	**Value**
Operating System	Windows 8.1 Pro, 64 bit
Drive type	SSD (Samsung 840 EVO)
CPU Type	Intel® Core(TM) i7-4930K
CPU Clock Rate	3.4 GHz
CPU RAM	32.0 GB
GPU Type	GeForce GTX TITAN Black
GPU Clock Rate	0.98 GHz
GPU RAM	6.0 GB
GPU Number of cores	2880

Table 2. Results from the efficiency test of the fast time-domain SAR processor.

Properties	**Case 1**	**Case 2**	**Case 3**	**Case 4**
Data-take duration [s]	87.3	82.1	107.6	92.4
Radar bandwidth [MHz]	600	600	600	300
Altitude AGL [m]	1210	1520	1830	1840
Ground pixel spacing [cm]	20	20	20	40
Illuminated area [km^2]	4.61	5.41	9.32	7.44
Total processing time [min]	45.8	57.8	103.6	32.0
Total areal processing rate [km^2/h]	6.35	5.62	5.39	13.93

4. DISCUSSION

A fast time-domain processor for focusing data from airborne FMCW SAR sensors was implemented and tested using real data. Its robustness was demonstrated using real SAR data-takes at Ka-band from highly non-linear trajectories and with a wide variety of swath geometries. An integrated relative radiometric correction yields enhanced imaging quality. Optional single- and multi-look processing as well as exo-clutter processing are also integrated in the processor, widening its possible applications.

The Point Target Analysis applied to the signatures of corner reflectors confirmed the high focusing quality as already seen from the visual appearance of SAR images. An areal processing rate as high as 6 km^2/h using 20 cm ground pixel spacing on a single PC station could be achieved.

Generally speaking, the obtained SAR processing efficiency is now that high that it typically makes it possible to process in high resolution all data-takes of one day of a measurement campaign overnight until the next day. More specific questions regarding the signatures of objects in predefined areas of interest can be answered within a few minutes. For experimental systems this is a relevant practical advantage for detecting potential troubles or for adjusting the system parameters or the flight conditions to the campaigns' goals.

Considerable efforts have already been put to speed-up the processor without quality loss. Further significant improvement is possible without major investment by using two GPUs, for which the required software adaption is expected to be relatively minor using the CUDA architecture.

REFERENCES

[1] Essen, H., Brehm, T., Haegelen, M. and Schimpf, H., "Remote Sensing at Millimetre Waves with the MEMPHIS Synthetic Aperture Radar," Proc. 7th European Conference on Synthetic Aperture Radar (Friedrichshafen, Germany), 1-4 (2008).

[2] Edrich, M. and Weiss, G., "Second-Generation Ka-Band UAV SAR System," Proc. 8th European Microwave Conference (Amsterdam, The Netherlands), 1636-1639 (2008).

[3] Stanko, S., Johannes, W., Sommer, R., Wahlen, A., Wilcke, J., Essen, H., Tessmann, A. and Kallfass, I., "SAR with MIRANDA - millimeterwave radar using analog and new digital approach," Proc. 8th European Radar Conference (Manchester, United Kingdom), 214-217 (2011).

[4] Stanko, S., Johannes, W., Sommer, R. and Wahlen, A., "SUMATRA - A miniaturized millimeter wave SAR," Proc. 14th International Radar Symposium (Dresden, Germany), 37-40 (2013).

[5] Meta, A., Lorga, J. F. M., de Wit, J. J. M. and Hoogeboom, P., "Motion compensation for a high resolution Ka-band airborne FM-CW SAR," Proc. 2nd European Radar Conference (Paris, France), 391-394 (2005).

[6] Ribalta, A., Roessing, L., Berens, P., Haegelen, M. and Wahlen, A., "High Resolution FMCW-SAR Image Generation," Proc. 8th European Conference on Synthetic Aperture Radar (Aachen, Germany), 1-4 (2010).

[7] Henke, D., Magnard, C., Frioud, M., Small, D., Meier E. and Schaepman, M. E., "Moving-Target Tracking in Single-Channel Wide-Beam SAR," IEEE Transactions on Geoscience and Remote Sensing, 50(11), 4735-4747 (2012).

[8] Frioud, M., Wahlen, A., Wellig, P. and Meier, E., "Processing of MIRANDA35 FMCW-SAR Data using a Time-Domain Algorithm," Proc. 10th European Conference on Synthetic Aperture Radar (Berlin, Germany), 85-88 (2014).

[9] Reigber, A., Scheiber, R., Jager, M., Prats-Iraola, P., Hajnsek, I., Jagdhuber, T., Papathanassiou, K. P., Nannini, M., Aguilera, E., Baumgartner, S., Horn, R., Nottensteiner, A. and Moreira, A., "Very-High-Resolution Airborne Synthetic Aperture Radar Imaging: Signal Processing and Applications," Proc. of the IEEE 101(3), 759-783 (2013).

[10] Johannes, W., Stanko, S., Wahlen, A., Sommer, R., Pohl, N., Wellig, P., Sennhauser, C., Meier, E. and Kallfass, I., "Implementation of a 35 GHz SAR sensor and a high resolution camera to enable real-time observation," Proc. 10th European Conference on Synthetic Aperture Radar (Berlin, Germany), 315-318 (2014).

[11] Palm, S., Wahlen, A., Stanko, S., Pohl, N., Wellig, P. and Stilla, U., "Real-Time Onboard Processing and Ground Based Monitoring of FMCW-SAR Videos," Proc. 10th European Conference on Synthetic Aperture Radar (Berlin, Germany), 89-92 (2014).